Observational constraints on the standard cosmological model and beyond

L. Sriramkumar

Department of Physics, Indian Institute of Technology Madras, Chennai

Workshop on Gravitational Waves

Chennai Mathematical Institute, Chennai

March 2–4, 2015

Plan of the talk

Ben Wandelt's cosmic cone

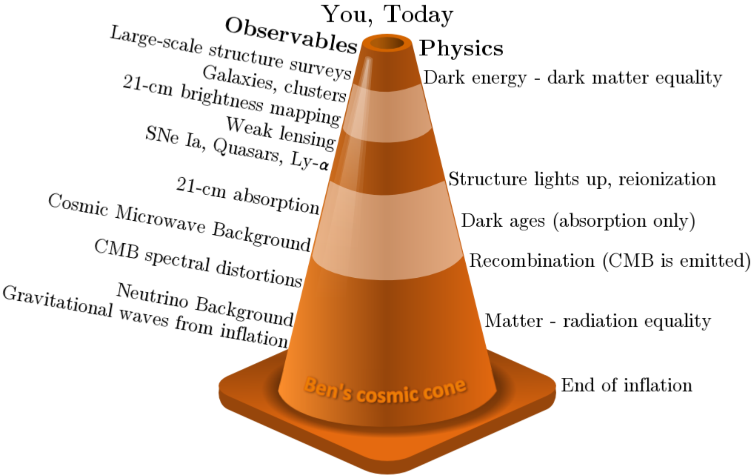

A schematic representation of the past light cone[1]. On the left are the cosmological observables, already observed or predicted. On the right are the physical phenomena they relate to, in the standard cosmological model.

[1] F. Leclercq, A. Pisani, B. D. Wandelt, arXiv:1403.1260 [astro-ph.CO].

Supernovae (SNe) and dark energy[2]

- SNe Ia remain, at present, the most direct and mature method of probing the dark energy due to several decades of intensive study and use in cosmology.
- Thought to be the result of the thermonuclear destruction of an accreting CO white dwarf star approaching the Chandrasekhar mass limit, they are standardizable candles which explode with nearly the same brightness everywhere in the universe due to the uniformity of the triggering mass and hence the available nuclear fuel.
- Their cosmological use exploits simple empirical relations between their luminosity and other parameters.

[2] M. Sullivan *et al.*, Astrophys. J. **737**, 102 (2011).

The Supernova Legacy Survey (SNLS)[3]

- The Canada-France-Hawaii Telescope (CFHT) Legacy Survey Supernova Program (SNLS) primary goal was to measure the equation of state of dark energy. It was designed to precisely measure several hundred Type Ia supernovae at redshifts between about 0.3 and unity.

The SNLS survey consisted of:

- A large imaging survey at CFHT: Between 2003 and 2008, the CFHT Legacy Survey detected and monitored about 1000 SNe.
- A large spectroscopic survey: About 500 high-redshift Type Ia SNe were observed on $8\,\mathrm{m}$ class telescopes (Gemini, VLT, Keck). The primary goal was to obtain supernova identification and redshift. Detailed spectroscopy of a subsample of distant SNe was also done to validate the use of Type Ia SNe as cosmological candles.

[3] See http://cfht.hawaii.edu/SNLS/.

A supernova explosion in a distant galaxy

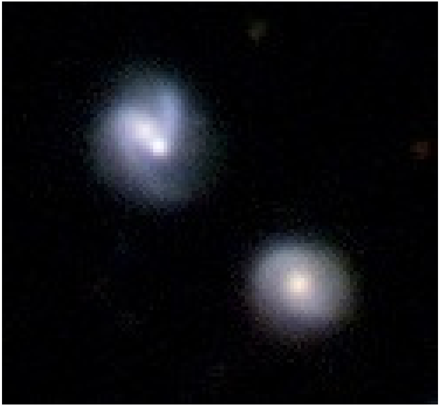
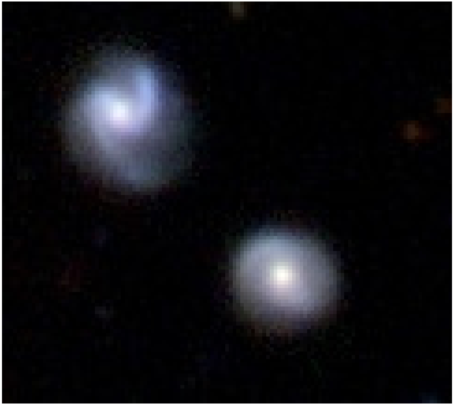

A supernova at $z = 0.28$ discovered by SNLS[4]. The supernova appears in the left image at maximum light and on the right is an image after the supernova has faded.

[4] C. J. Pritchet *et al.*, arXiv:astro-ph/0406242.

SNLS3 and other data sets[5]

- The SNe Ia samples are divided into two categories: those discovered and confirmed by SNLS, and those taken from the literature which sample different redshift ranges to SNLS.
- The complete data set consists of 242 well-sampled SNe Ia over $0.08 < z < 1.06$ from the SNLS together with a large literature sample: 123 SNe Ia at low-redshift, 14 SNe Ia at $z \gtrsim 0.8$ from the Hubble Space Telescope, and 93 SNe Ia at intermediate redshift from the first year of the SDSS-II SN search.
- The advantages of the enlarged SNLS data set are multiple. Most obviously, this represents a threefold increase in the SNLS sample size compared to the first year SNLS cosmological analysis, and as such provides a significant improvement in the statistical precision of the cosmological constraints.
- Moreover, the enlarged data set allows sources of potential astrophysical systematics to be examined by dividing our SN Ia sample according to properties of either the SN or its environment.

[5] M. Sullivan *et al.*, Astrophys. J. **737**, 102 (2011).

Constraints on the background parameters[6]

All the results from SNLS3 are consistent with a spatially flat, $w = -1$ universe.

The results for a flat universe with a constant dark energy equation of state are

$$\begin{aligned} \Omega_{\rm m} &= 0.269 \pm 0.015, \\ w &= -1.061^{+0.069}_{-0.068}, \end{aligned}$$

and, relaxing the assumption of spatial flatness,

$$\begin{aligned} \Omega_{\rm m} &= 0.271 \pm 0.015, \\ \Omega_k &= -0.002 \pm 0.006, \\ w &= -1.069^{+0.091}_{-0.092}, \end{aligned}$$

including external constraints from WMAP7 and SDSS DR7 and a prior on H_0.

[6] M. Sullivan *et al.*, Astrophys. J. **737**, 102 (2011).

Constraints in the spatially flat case

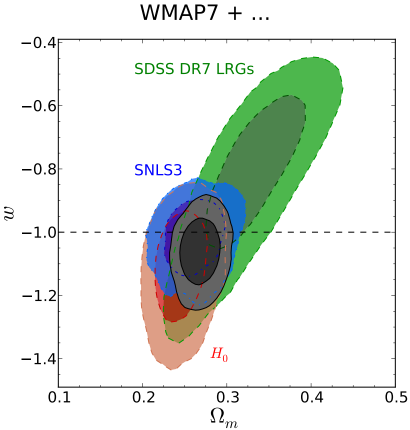

Confidence contours on the cosmological parameters $\Omega_{\rm m}$ and w assuming a flat universe, produced using the CosmoMC program[7]. The SNLS3 contours are in blue, the SDSS DR7 LRG contours in green, and the H_0 prior in red. WMAP7 constraints are included in all contours. The combined constraints are shown in grey.

[7] M. Sullivan *et al.*, Astrophys. J. **737**, 102 (2011).

Constraints in the non-flat case

WMAP7 + ...

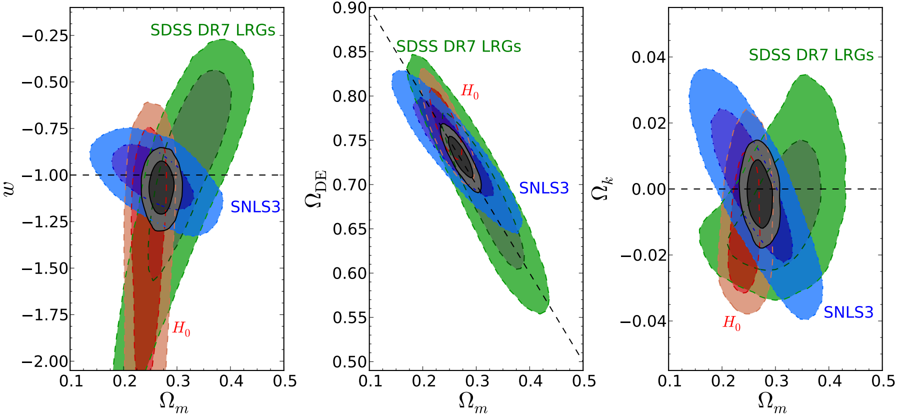

Confidence contours on the cosmological parameters $\Omega_{\rm m}$, $\Omega_{\rm DE}$, Ω_k, and w, with the same choice of colors to represent the different data sets as in the previous figure[8].

[8] M. Sullivan *et al.*, Astrophys. J. **737**, 102 (2011).

Parameterizing the variation in dark energy

The variation in the dark energy is usually parametrized as[9]

$$w(a) = w_0 + w_a\,(1-a),$$

with the cosmological constant being equivalent to $w_0 = 1$ and $w_a = 0$.

Upon assuming a spatially flat universe, the best fit values and the 1-σ deviations of the parameters $(\Omega_{\rm m}, w_0, w_a)$ prove to be[10]

$$\begin{aligned}\Omega_{\rm m} &= 0.271^{+0.015}_{-0.015},\\ w_0 &= -0.905^{+0.196}_{-0.196},\\ w_a &= -0.984^{+1.094}_{-1.097}.\end{aligned}$$

In other words, there is no evidence for a deviation from the cosmological constant.

[9] M. Chevallier and D. Polarski, Int. J. Mod. Phys. D, **10**, 213 (2001);
E. V. Linder, E. V. 2003, Phys. Rev. Lett. **90**, 091301 (2003).

[10] M. Sullivan *et al.*, Astrophys. J. **737**, 102 (2011).

Constraints on the variation in dark energy

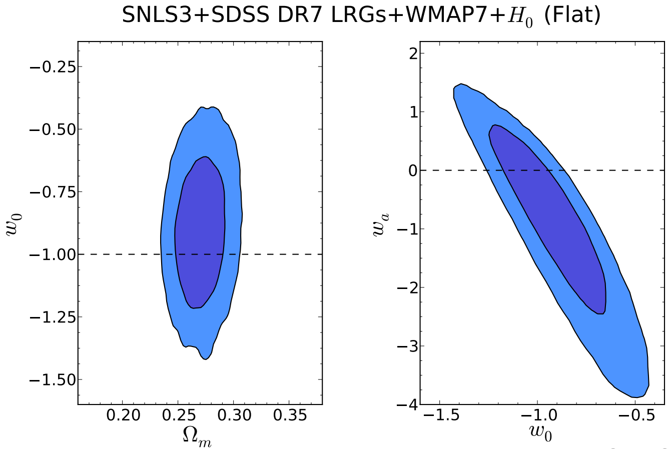

Combined confidence contours in $\Omega_{\rm m}$, w_0 and w_a using SNLS3, WMAP7, SDSS DR7 LRGs, and a prior on H_0. A flat universe is assumed, and a prior of $w_0 + w_a \leq 0$ has been enforced—any apparent discrepancy with this prior is a result of smoothening the CosmoMC output[11].

[11] M. Sullivan *et al.*, Astrophys. J. **737**, 102 (2011).

The dark energy survey

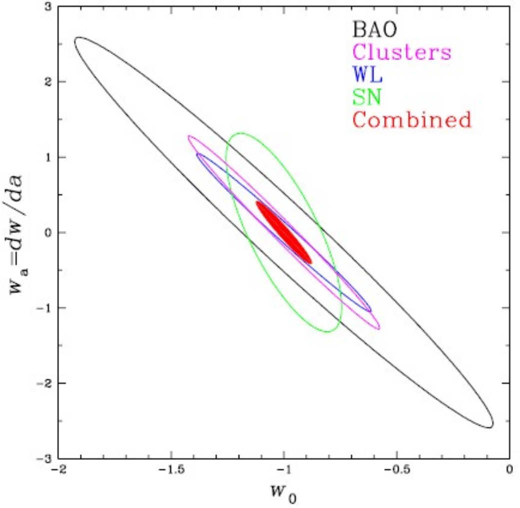

Expected constraints from the dark energy survey[12].

[12] From https://www.darkenergysurvey.org/reports/proposal-standalone.pdf.

The Planck mission

- Planck's scientific payload contained an array of 74 detectors in nine frequency bands sensitive to frequencies between 25 and $1000\,\mathrm{GHz}$, which scanned the sky with angular resolution between $33'$ and $5'$.
- Planck had carried a Low Frequency Instrument (LFI) and a High Frequency Instrument (HFI). The detectors of the LFI were pseudo-correlation radiometers, covering bands centered at 30, 44, and $70\,\mathrm{GHz}$. The detectors of the HFI were bolometers, covering bands centered at 100, 143, 217, 353, 545, and $857\,\mathrm{GHz}$.
- Planck imaged the whole sky twice in one year, with a combination of sensitivity, angular resolution, and frequency coverage never before achieved.

CMB anisotropies as seen by Planck

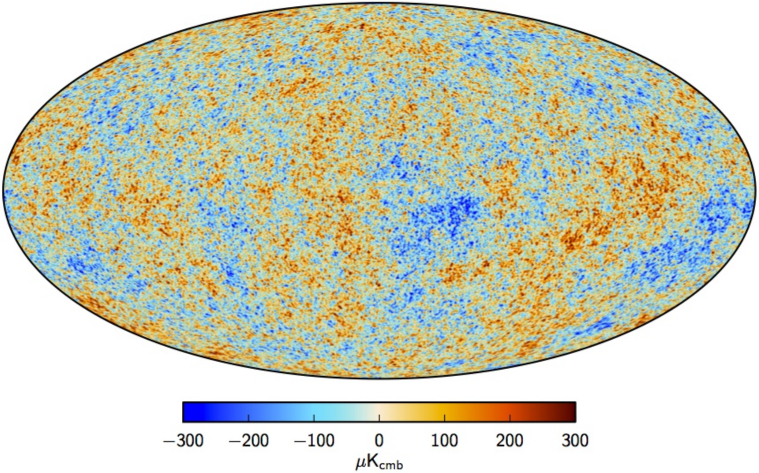

CMB intensity map at $5'$ resolution derived from the joint analysis of Planck, WMAP, and $408\,\mathrm{MHz}$ observations[13].

[13] P. A. R. Ade *et al.*, arXiv:1502.01582 [astro-ph.CO].

CMB TT angular power spectrum from Planck[14]

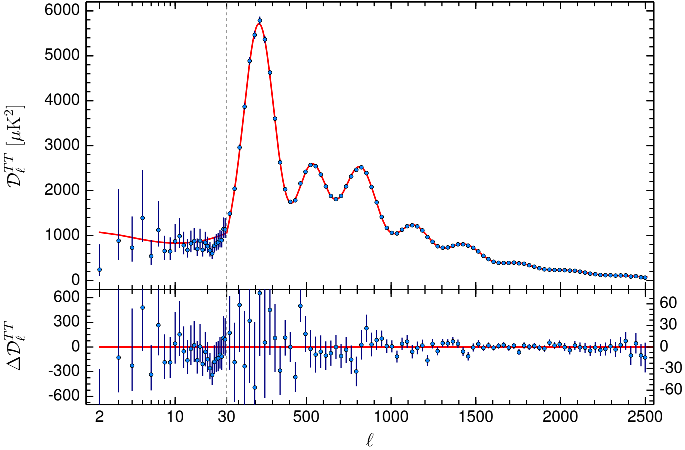

The CMB TT angular power spectrum from the Planck 2015 data (the blue dots with error bars) and the theoretical, best fit ΛCDM model with a power law primordial spectrum (the solid red curve).

[14] P. A. R. Ade *et al.*, arXiv:1502.02114 [astro-ph.CO].

CMB TE and EE angular power spectra from Planck[15]

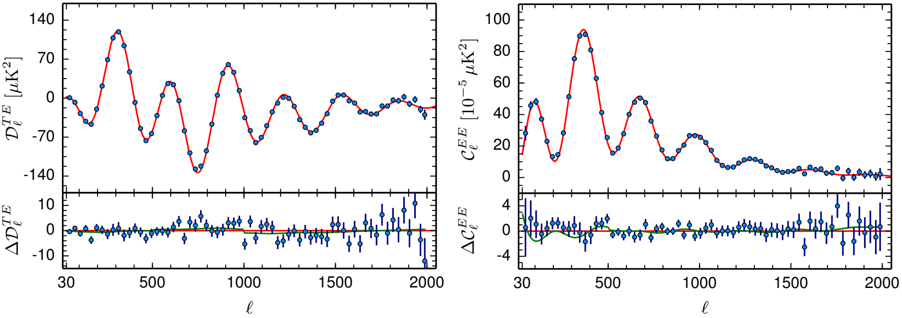

The CMB TE (on the left) and EE (on the right) angular power spectra from the Planck 2015 data (the blue dots with error bars) and the theoretical, best fit ΛCDM model with a power law primordial spectrum (the solid red curves).

[15] P. A. R. Ade *et al.*, arXiv:1502.02114 [astro-ph.CO].

Best fit values of the cosmological parameters[16]

Parameter	TT+lowP	TT+lowP+lensing	TT+lowP+BAO	TT,TE,EE+lowP
$\Omega_{\mathrm{b}}h^2$	0.02222 ± 0.00023	0.02226 ± 0.00023	0.02226 ± 0.00020	0.02225 ± 0.00016
$\Omega_{\mathrm{c}}h^2$	0.1197 ± 0.0022	0.1186 ± 0.0020	0.1190 ± 0.0013	0.1198 ± 0.0015
$100\theta_{\mathrm{MC}}$	1.04085 ± 0.00047	1.04103 ± 0.00046	1.04095 ± 0.00041	1.04077 ± 0.00032
τ	0.078 ± 0.019	0.066 ± 0.016	0.080 ± 0.017	0.079 ± 0.017
$\ln(10^{10}A_{\mathrm{s}})$	3.089 ± 0.036	3.062 ± 0.029	3.093 ± 0.034	3.094 ± 0.034
n_{s}	0.9655 ± 0.0062	0.9677 ± 0.0060	0.9673 ± 0.0045	0.9645 ± 0.0049
H_0	67.31 ± 0.96	67.81 ± 0.92	67.63 ± 0.57	67.27 ± 0.66
Ω_{m}	0.315 ± 0.013	0.308 ± 0.012	0.3104 ± 0.0076	0.3156 ± 0.0091

Confidence limits on the parameters of the base ΛCDM model, for various combinations of the Planck 2015 data, at the 68% confidence level.

[16] P. A. R. Ade *et al.*, arXiv:1502.02114 [astro-ph.CO].

Tension regarding H_0

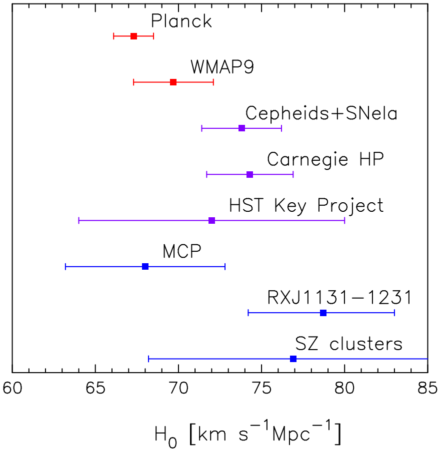

Comparison of the H_0 measurements, with estimates of ± 1-σ errors, from a number of techniques[17]. These are compared with the spatially flat ΛCDM model constraints from Planck and WMAP9.

[17] P. A. R. Ade *et al.*, arXiv:1303.5076 [astro-ph.CO].

Why is the CMB relevant for dark energy?[18]

1. Change the expansion history and hence distance to the last scattering surface, with a shift in the peaks, sometimes referred to as a geometrical projection effect
2. Cause the decay of gravitational potentials at late times, affecting the low-multipole CMB anisotropies through the integrated Sachs-Wolfe (ISW) effect
3. Enhance the cross-correlation between the CMB and large-scale structure, through the ISW effect
4. Change the lensing potential, through additional DE perturbations or modifications of GR
5. Modify the lensing B-mode contribution, through changes in the lensing potential
6. Modify the primordial B-mode amplitude and scale dependence, by changing the sound speed of gravitational waves

[18] P. A. R. Ade *et al.*, arXiv:1502.01590 [astro-ph.CO].

Constraints on the dark energy parameters

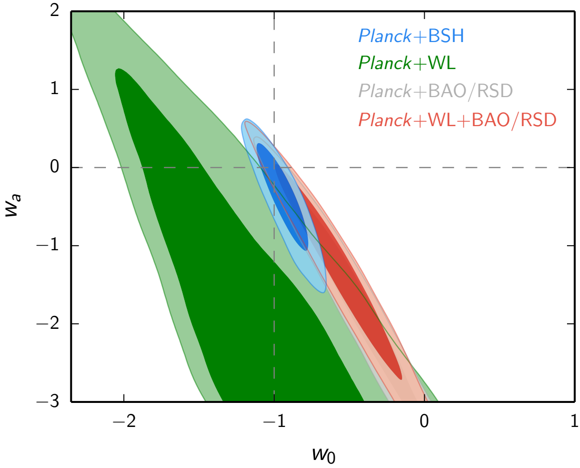

Marginalized posterior distributions of the (w_0,w_a) parameterization for various data combinations[19].

[19] P. A. R. Ade *et al.*, arXiv:1502.01590 [astro-ph.CO].

Evolution of the equation of state[20]

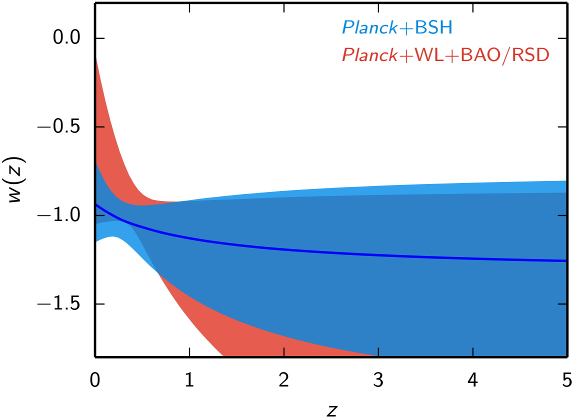

Reconstructed equation of state $w(z)$ as a function of redshift, when assuming a Taylor expansion of $w(z)$ to first order, for different combinations of the data sets. The colored areas show the regions which contain $95\,\%$ of the models.

[20] P. A. R. Ade *et al.*, arXiv:1502.01590 [astro-ph.CO].

The scalar spectral index and running[21]

For the base ΛCDM model with a power law power spectrum of curvature perturbations, the constraint on the scalar spectral index, $n_{\rm s}$, with the Planck full mission temperature data is

$$n_{\rm s} = 0.9655 \pm 0.0062 \ \ (68\,\%\ \text{CL, Planck TT + low P}).$$

The running of the scalar spectral index is constrained by the Planck 2015 full mission temperature data to

$$\frac{{\rm d}n_{\rm s}}{{\rm d}\ln k} = -0.0084 \pm 0.0082 \ \ (68\,\%\ \text{CL, Planck TT + low P}).$$

The combined constraint including high-ℓ polarization is

$$\frac{{\rm d}n_{\rm s}}{{\rm d}\ln k} = -0.0057 \pm 0.0071 \ \ (68\,\%\ \text{CL, Planck TT, TE, EE + low P}).$$

Adding the Planck CMB lensing data to the temperature data further reduces the central value for the running, i.e. ${\rm d}n_{\rm s}/{\rm d}\ln k = -0.0033 \pm 0.0074$ ($68\,\%$ CL, Planck TT + low P+ lensing).

[21] P. A. R. Ade *et al.*, arXiv:1502.02114 [astro-ph.CO].

Joint constraints on the spectral index and running[22]

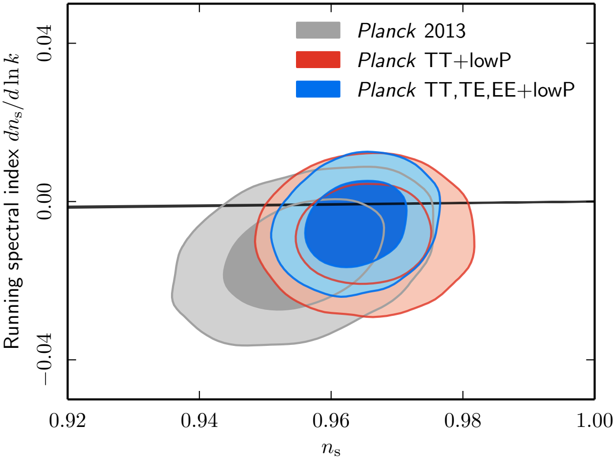

Marginalized joint $68\,\%$ and $95\,\%$ CL for $(n_{\rm s}, {\rm d}n_{\rm s}/{\rm d}\ln k)$ using Planck TT + low P and Planck TT, TE, EE + low P. The thin black stripe shows the prediction for single field monomial chaotic inflationary models with $50 < N_* < 60$.

[22] P. A. R. Ade *et al.*, arXiv:1502.02114 [astro-ph.CO].

Constraints on the tensor-to-scalar ratio r [23]

The constraints on the tensor-to-scalar ratio inferred from the Planck full mission data for the ΛCDM + r model are:

$$
\begin{aligned}
r_{0.002} &< 0.10 \ (95\,\% \text{ CL, Planck TT + low P}),\\
r_{0.002} &< 0.11 \ (95\,\% \text{ CL, Planck TT + low P + lensing}),\\
r_{0.002} &< 0.11 \ (95\,\% \text{ CL, Planck TT + low P + BAO}),\\
r_{0.002} &< 0.10 \ (95\,\% \text{ CL, Planck TT, TE, EE + low P}).
\end{aligned}
$$

[23] P. A. R. Ade *et al.*, arXiv:1502.02114 [astro-ph.CO].

Spectral index and running with tensors[24]

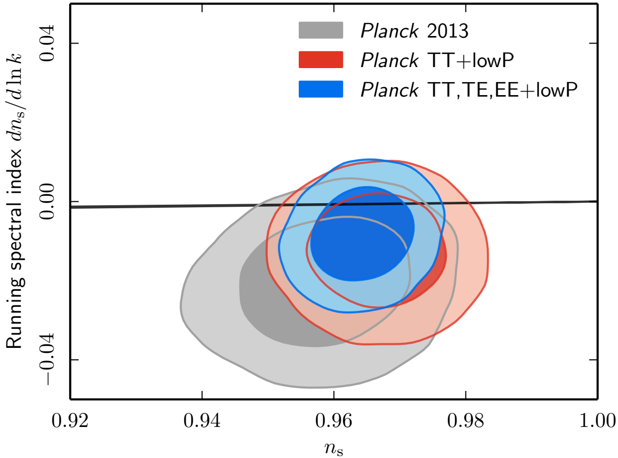

Marginalized joint confidence contours for $(n_{\rm s}, {\rm d}n_{\rm s}/{\rm d}\ln k)$, at the $68\,\%$ and $95\,\%$ CL, in the presence of a non-zero tensor contribution, and using Planck TT + low P or Planck TT, TE, EE + low P.

[24] P. A. R. Ade *et al.*, arXiv:1502.02114 [astro-ph.CO].

Joint constraints on r and ns[25]

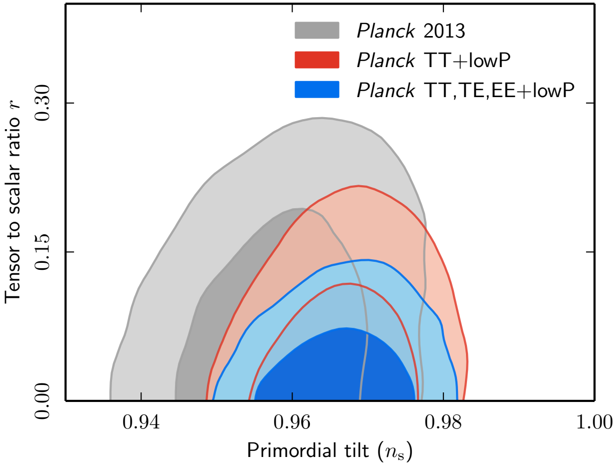

Marginalized joint confidence contours for $(n_{\rm s}, r)$, at the $68\,\%$ and $95\,\%$ CL, in the presence of running of the spectral indices, and for the same combinations of data as in the previous figure.

[25] P. A. R. Ade *et al.*, arXiv:1502.02114 [astro-ph.CO].

Constraints on the slow roll parameters[26]

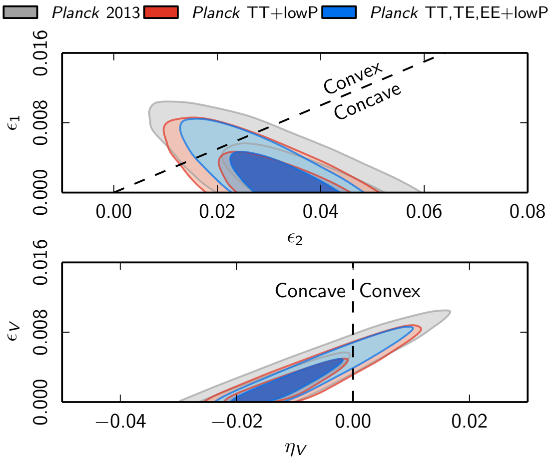

Joint $68\,\%$ and $95\,\%$ CL regions for (ϵ_1, ϵ_2) (top panel) and $(\epsilon_{\rm V}, \eta_{\rm V})$ (bottom panel) for Planck TT + low P (red contours), Planck TT, TE, EE + low P (blue contours), and compared with the Planck 2013 results (grey contours).

[26] P. A. R. Ade *et al.*, arXiv:1502.02114 [astro-ph.CO].

Performance of models in the n_s-r plane[27]

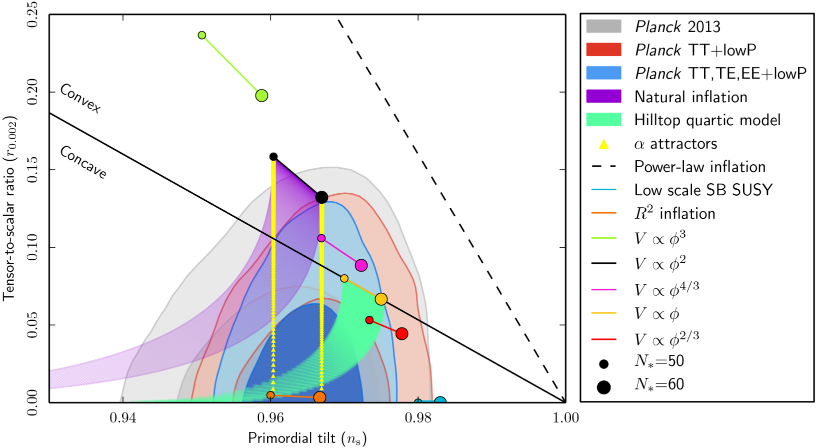

Marginalized joint $68\,\%$ and $95\,\%$ CL regions for n_s and $r_{0.002}$ from Planck in combination with other data sets, compared to the theoretical predictions of selected inflationary models.

[27] P. A. R. Ade *et al.*, arXiv:1502.02114 [astro-ph.CO].

Constraints upon inclusion of BICEP data[28]

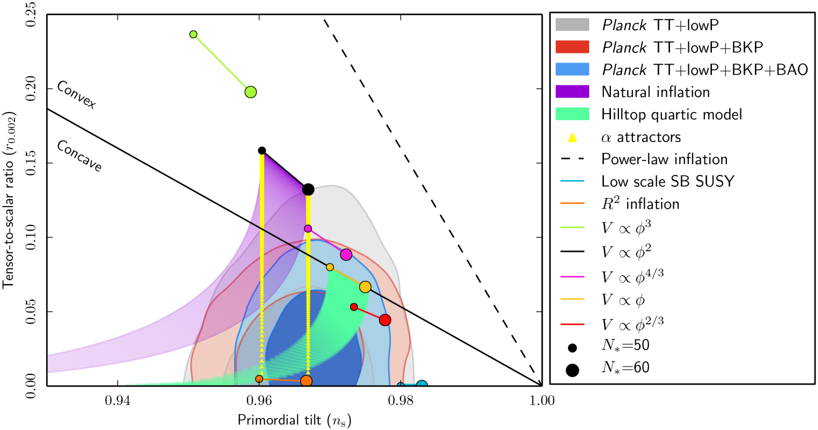

Marginalized joint $68\,\%$ and $95\,\%$ CL regions for n_s and $r_{0.002}$ from Planck alone and in combination with its cross-correlation with BICEP2/Keck Array and/or BAO data compared with the theoretical predictions of selected inflationary models.

[28] P. A. R. Ade *et al.*, arXiv:1502.02114 [astro-ph.CO].

Power spectra with features[29]

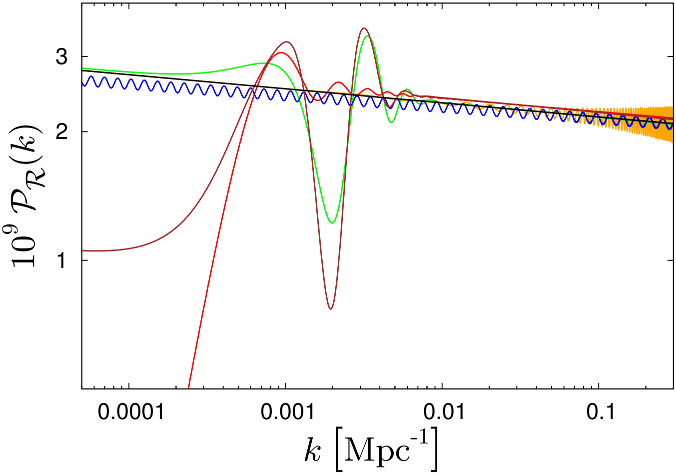

Primordial power spectra with features that lead to an improved fit to the data than the conventional, nearly scale, invariant spectra.

[29] P. A. R. Ade *et al.*, arXiv:1502.02114 [astro-ph.CO].

Template bispectra

For comparison with the observations, the scalar bispectrum is often expressed in terms of the parameters $f_{\rm NL}^{\rm loc}$, $f_{\rm NL}^{\rm eq}$ and $f_{\rm NL}^{\rm orth}$ as follows:

$$G_{\mathcal{R}\mathcal{R}\mathcal{R}}(\boldsymbol{k}_1,\boldsymbol{k}_2,\boldsymbol{k}_3) = f_{\rm NL}^{\rm loc}\, G_{\mathcal{R}\mathcal{R}\mathcal{R}}^{\rm loc}(\boldsymbol{k}_1,\boldsymbol{k}_2,\boldsymbol{k}_3) + f_{\rm NL}^{\rm eq}\, G_{\mathcal{R}\mathcal{R}\mathcal{R}}^{\rm eq}(\boldsymbol{k}_1,\boldsymbol{k}_2,\boldsymbol{k}_3) + f_{\rm NL}^{\rm orth}\, G_{\mathcal{R}\mathcal{R}\mathcal{R}}^{\rm orth}(\boldsymbol{k}_1,\boldsymbol{k}_2,\boldsymbol{k}_3).$$

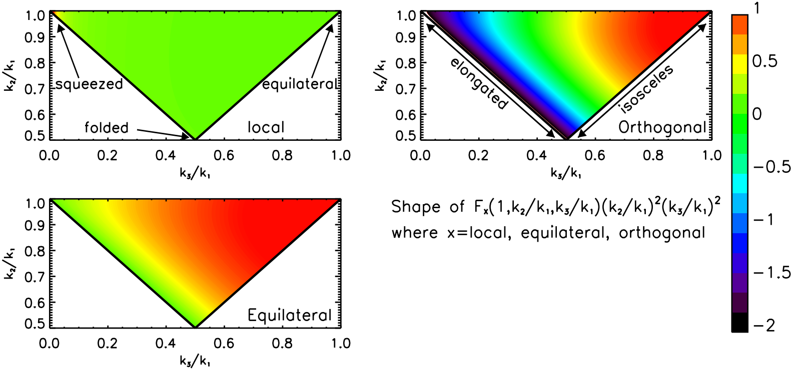

Illustration of the three template basis bispectra[30].

[30] E. Komatsu, Class. Quantum Grav. **27**, 124010 (2010).

The theoretical CMB TTT angular bispectrum

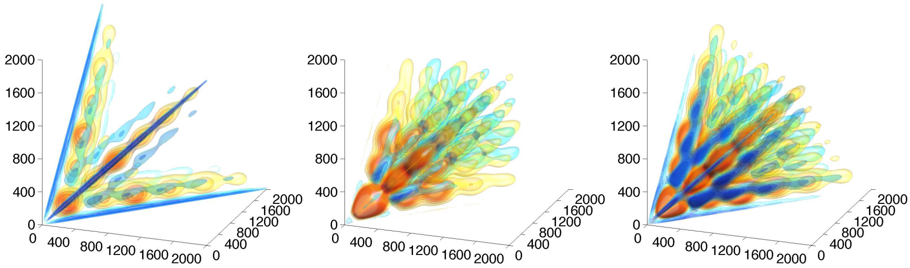

Theoretical predictions for the reduced bispectrum of the CMB, with inflationary models involving non-Gaussianities of local (left), equilateral (center) and orthogonal (right) type[31].

[31] F. Leclercq, A. Pisani, B. D. Wandelt, arXiv:1403.1260 [astro-ph.CO].

The observed CMB TTT angular bispectrum

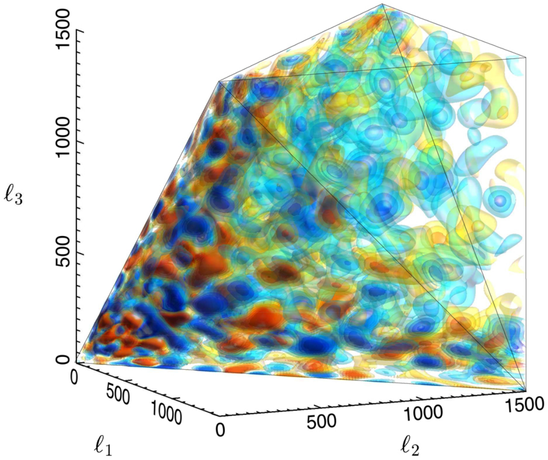

The CMB TTT angular bispectrum, as observed by Planck[32].

[32] P. A. R. Ade *et al.*, arXiv:1502.01592 [astro-ph.CO].

Constraints on the scalar non-Gaussianity parameters

The constraints on the primordial values of the non-Gaussianity parameters from the Planck data are as follows[33]:

$$
\begin{aligned}
f_{\rm NL}^{\rm loc} &= 0.8 \pm 5.0,\\
f_{\rm NL}^{\rm eq} &= -4 \pm 43,\\
f_{\rm NL}^{\rm orth} &= -26 \pm 21.
\end{aligned}
$$

These constraints imply that slowly rolling single field models involving the canonical scalar field which are favored by the data at the level of power spectra are also consistent with the data at the level of non-Gaussianities.

[33] P. A. R. Ade *et al.*, arXiv:1502.01592 [astro-ph.CO].

Constraints on the neutrino masses

The constraints on the sum of the neutrino masses, assuming three species of degenerate massive neutrinos, are as follows[34]:

$$\sum m_\nu < 0.72\,\mathrm{eV} \quad (95\,\% \text{ CL, Planck TT + low P}),$$
$$\sum m_\nu < 0.21\,\mathrm{eV} \quad (95\,\% \text{ CL, Planck TT + low P + BAO}),$$
$$\sum m_\nu < 0.49\,\mathrm{eV} \quad (95\,\% \text{ CL, Planck TT, TE, EE + low P}),$$
$$\sum m_\nu < 0.17\,\mathrm{eV} \quad (95\,\% \text{ CL, Planck TT, TE, EE + low P + BAO}).$$

[34] P. A. R. Ade *et al.*, arXiv:1502.01589 [astro-ph.CO].

Constraints on the number of relativistic species

The constraints on the sum of the number of relativistic species are as follows[35]:

$$
\begin{aligned}
N_{\rm eff} &= 3.13 \pm 0.32 \ \ (68\,\% \text{ CL, Planck TT + low P}),\\
N_{\rm eff} &= 3.15 \pm 0.23 \ \ (68\,\% \text{ CL, Planck TT + low P + BAO}),\\
N_{\rm eff} &= 2.99 \pm 0.20 \ \ (68\,\% \text{ CL, Planck TT, TE, EE + low P}),\\
N_{\rm eff} &= 3.04 \pm 0.18 \ \ (68\,\% \text{ CL, Planck TT, TE, EE + low P + BAO}).
\end{aligned}
$$

A significant density of additional radiation still seems to be allowed.

[35] P. A. R. Ade *et al.*, arXiv:1502.01589 [astro-ph.CO].

Baryon Acoustic Oscillations (BAO)

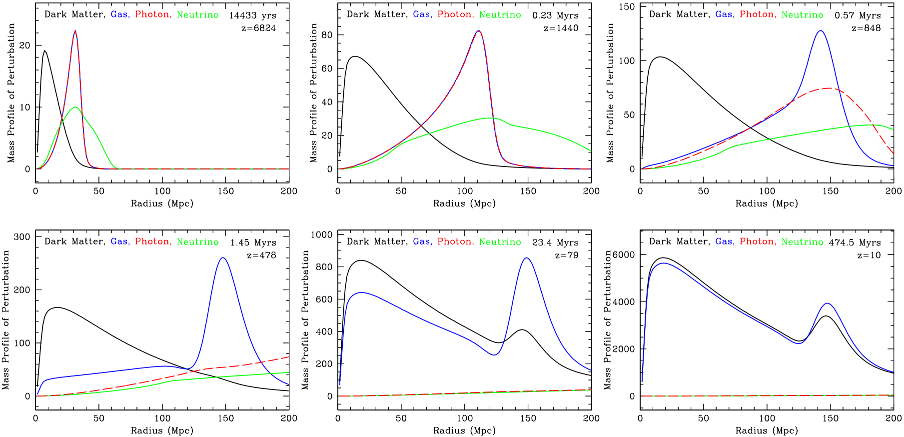

Snapshots of an evolving spherical density perturbation before and after decoupling[36].

---

[36] D. J. Eisenstein, H.-J. Seo and M. White, Astrophys. J. **664**, 660 (2007), B. A. Bassett and R. Hlozek, arXiv:0910.5224 [astro-ph.CO].

The scale of BAO

The BAO are frozen relics left over from the pre-decoupling universe.

The scale of BAO is set by the comoving size of the sound horizon at decoupling, which is given by

$$r_{\rm s} = \frac{c}{\sqrt{3}} \int\limits_0^{t_{\rm dec}} \frac{{\rm d}t}{a(t)}.$$

For $z_{\rm dec} \simeq 1100$, one finds that $r_{\rm s} \simeq 150\,{\rm Mpc}$.

One finds that the sound horizon can be approximated, around the WMAP5 best-fit location as[37]

$$r_s(z_d) = 153.5\,\left(\frac{\Omega_{\rm b}\,h^2}{0.02273}\right)^{-0.134}\,\left(\frac{\Omega_{\rm m}\,h^2}{0.1326}\right)^{-0.255}\,{\rm Mpc}.$$

[37] E. Komatsu *et al.*, Astrophys. J. Suppl. **180**, 330 (2009).

BAO in real space[38]

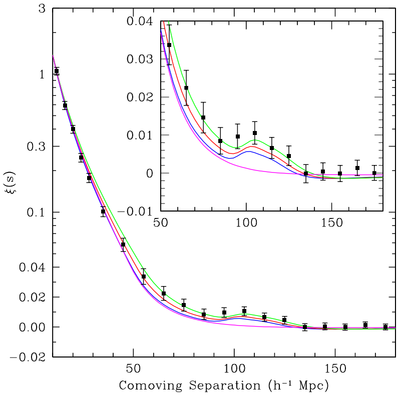

The Baryon Acoustic Peak (BAP) in the correlation function—the BAP is visible in the clustering of the SDSS LRG galaxy sample, and is sensitive to the matter density [shown are models with $\Omega_{\mathrm{m}}\, h^2 = 0.12$ (top), 0.13 (second) and 0.14 (third), all with $\Omega_{\mathrm{b}}\, h^2 = 0.024$]. The bottom line without a BAP is the correlation function in the pure CDM model, with $\Omega_{\mathrm{b}} = 0$.

[38] D. J. Eisenstein *et al.*, Astrophys. J. **633**, 560 (2005).

BAO in the WiggleZ survey

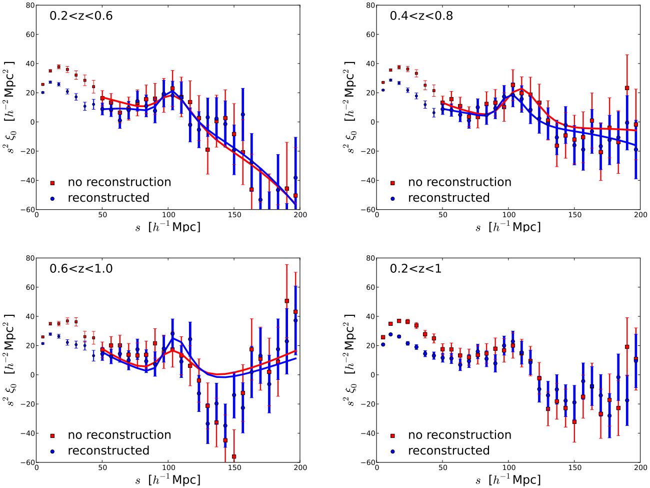

The WiggleZ two-point correlation functions (red squares) for three redshifts bins and the full z range. These are plotted as $\xi\, s^2$ to emphasize the feature[39].

[39] E. A. Kazin *et al.*, Mon. Not. Roy. Astron. Soc. **441**, 3524 (2014).

Fourier pairs $\xi(r)$ and $P(k)$

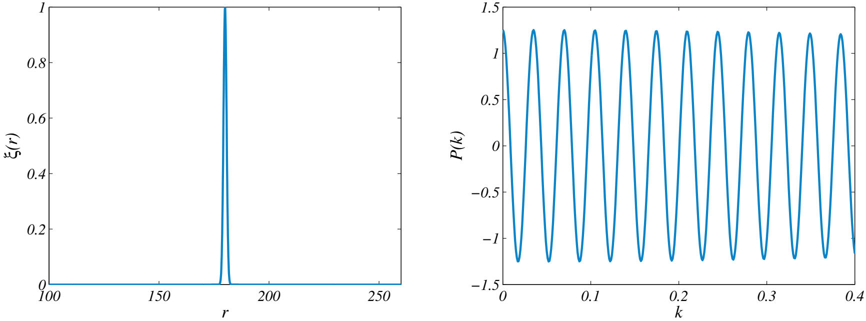

Schematic illustration of the Fourier pairs $\xi(r)$ and $P(k)$. A sharp peak in the correlation function (left panel) corresponds to a series of oscillations in the power spectrum (right panel). The BAP in the correlation function will induce characteristic BAO in the power spectrum[40].

[40] B. A. Bassett and R. Hlozek, arXiv:0910.5224 [astro-ph.CO].

BAO in Fourier space[41]

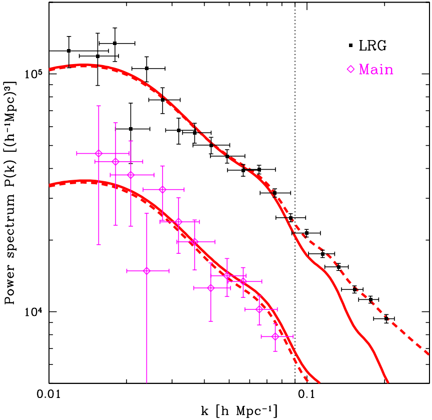

BAO in the SDSS power spectra—the BAP of the previous figure now becomes a series of oscillations in the matter power spectrum of the SDSS sample. The solid lines show the ΛCDM fits to the WMAP3 data, while the dashed lines include nonlinear corrections.

[41] M. Tegmark *et al.*, Phys. Rev. D **74**, 123507 (2006).

BAO in the SDSS power spectra[42]

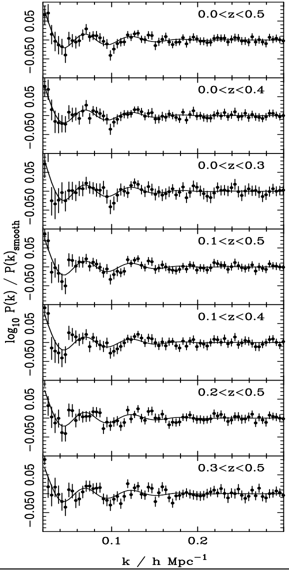

BAO recovered from the SDSS Data (release 7 galaxy sample) for each of the redshifts slices (solid circles with 1-σ error bars). These are compared with BAO in the default ΛCDM model (solid lines).

[42] W. Percival *et al.*, arXiv:0907.1660 [astro-ph.CO].

BAO as a standard ruler

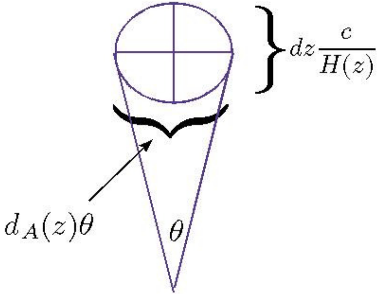

The radial length of an object is given by $c\,\mathrm{d}z/H(z)$ where $\mathrm{d}z$ is the difference in redshift between the front and back of the object, while the transverse size of the object is $d_{\mathrm{A}}(z)\,\theta$ and θ is its angular size. If one knows that the object is spherical (but does not know the actual diameter), then one can determine the product $d_{\mathrm{A}}(z)\,H(z)$ from measuring $\mathrm{d}z/\theta$. If, as in the case of BAO, one can theoretically determine the diameter, one has the bonus of finding $d_{\mathrm{A}}(z)$ and $H(z)$ separately[43].

[43] B. A. Bassett and R. Hlozek, arXiv:0910.5224 [astro-ph.CO].

BAO surveys

BAO surveys measure the distance ratio

$$d_z = \frac{r_{\rm s}(z_{\rm drag})}{D_{\rm V}(z)},$$

where $r_{\rm s}(z_{\rm drag})$ is the comoving sound horizon at the baryon drag epoch (when baryons became dynamically decoupled from the photons) and $D_{\rm V}(z)$ is a combination of the angular diameter distance, $d_{\rm A}(z)$, and the Hubble parameter, $H(z)$, appropriate for the analysis of spherically-averaged two-point statistics:

$$D_{\rm V}(z) = \left[\frac{(1+z)^2\, d_{\rm A}^2(z)\, c\, z}{H(z)}\right]^{1/3}.$$

Constraints from WiggleZ

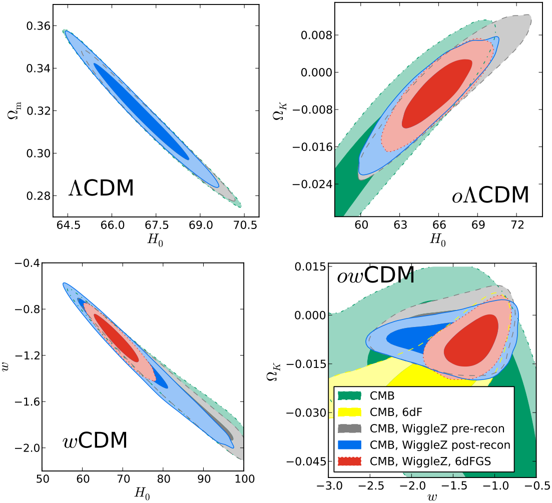

Marginalized joint confidence regions of cosmological parameter pairs from the WiggleZ survey and the CMB (Planck 2013 + WMAP9 polarization) data[44].

[44] E. A. Kazin *et al.*, Mon. Not. Roy. Astron. Soc. **441**, 3524 (2014).

Constraints from BAO surveys and Planck

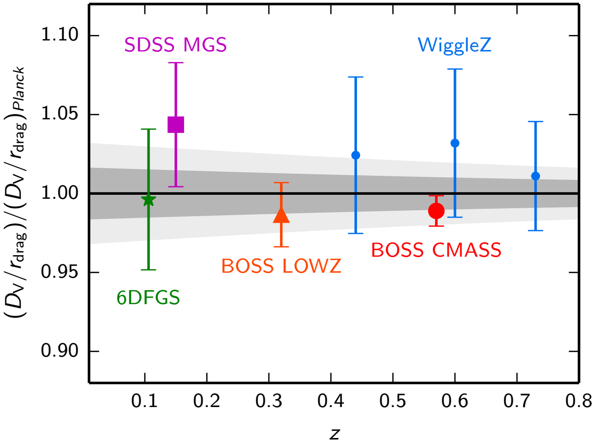

Acoustic scale distance ratio $r_s/D_V(z)$ divided by the distance ratio of the Planck base ΛCDM model[45]. The grey bands shows the approximate 68% and 95% ranges allowed by Planck.

[45] P. A. R. Ade *et al.*, arXiv:1502.01589 [astro-ph.CO].

Hemispherical asymmetry: Prior to Planck

- With the first year WMAP data, it was discovered that the angular power spectrum, when estimated locally at different positions on the sphere, appears not to be isotropic[46].
- In particular, the power spectrum calculated for a hemisphere centered at $(\theta, \phi) = (110°, 237°)$ (in galactic co-latitude and longitude) was larger than when calculated in the opposite hemisphere over the multipole range $\ell = 2$–40.

[46] H. K. Eriksen, F. K. Hansen, A. J. Banday, K. M. Gorski and P.B. Lilje, Astrophys. J. **605**, 14 (2004); F. K. Hansen, A. J. Banday and K. M. Gorski, Mon. Not. Roy. Astron. Soc. **354**, 641 (2004).

Hemispherical asymmetry: Planck 2013

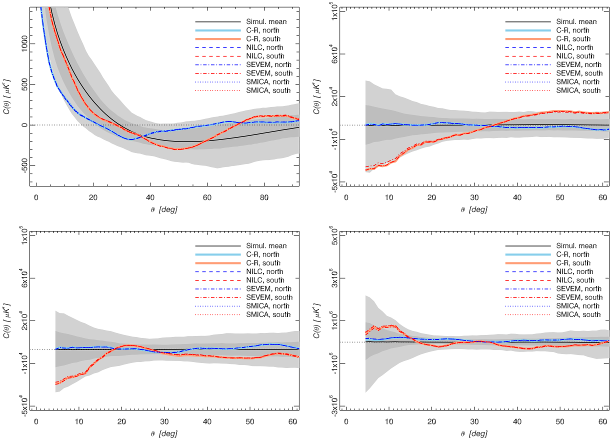

The two-point (upper left), pseudo-collapsed (upper right), equilateral three-point (lower left), and rhombic four-point (lower right) correlation functions ($N_{\rm side} = 64$). Correlation functions are shown for the analysis performed on northern (blue) and southern (red) hemispheres determined in the ecliptic coordinate frame[47].

[47] P. A. R. Ade *et al.*, arXiv:1303.5083 [astro-ph.CO].

The distance-duality relation

In any metric theory of gravity, the luminosity distance $d_{\mathrm{L}}(z)$ and the angular diameter distance $d_{\mathrm{A}}(z)$ are related as follows[48]:

$$d_{\mathrm{L}}(z) = (1+z)^2\, d_{\mathrm{A}}(z).$$

While this relation is impervious to gravitational lensing, it depends crucially on photon conservation. The distance-duality relation can become a powerful test of a wide range of both exotic and fairly mundane physics[49].

[48] J. M. H. Etherington, Phil. Mag. **15**, 761 (1933).

[49] B. A. Bassett and M. Kunz, Phys. Rev. D **69**, 101305 (2014).

Constraints on the distance-duality relation

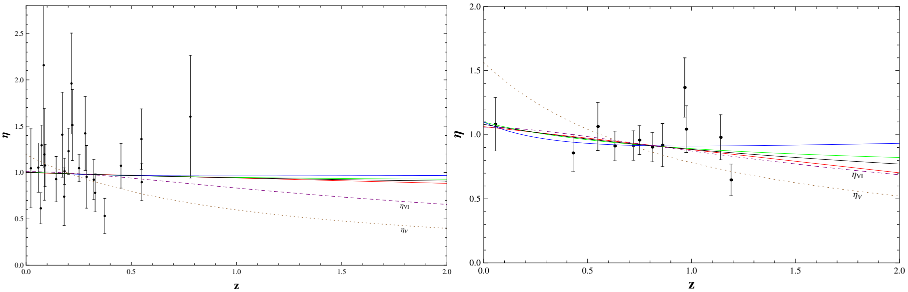

Constraints on the ratio $\eta(z) = d_{\rm L}/[d_{\rm A}\,(1+z)^2]$ from the supernovae and the BAO data[50].

[50] R. Nair, S. Jhingan and D. Jain, JCAP **1105**, 023 (2011).

The growth rate

The growth rate $f(z)$ is defined through the relation[51]

$$f(z) = \frac{\mathrm{d} \ln \delta}{\mathrm{d} \ln a},$$

where $\delta(a)$ denotes the perturbation in the dark matter.

Recall that, in the matter dominated epoch, $\delta \propto a$.

[51] See, for instance, M. J. Mortonson, D. H. Weinberg and M. White, arXiv:1401.0046 [astro-ph.CO].

The growth index

The so-called growth index γ is defined through the relation[52]

$$g(a) = \exp \int \mathrm{d} \ln a \; [\Omega_m^{\gamma}(a) - 1] \, ,$$

where $g = \delta(a)/a$, with δ denoting the perturbation in the dark matter. Within general relativity and in the standard ΛCDM model, it is found that $\gamma \simeq 0.55$.

The growth rate is known to be different when there is variation in the dark energy and in different models of gravity.

[52] E. V. Linder, Phys. Rev. D **72**, 043529 (2005).

Constraints from Euclid on the growth rate

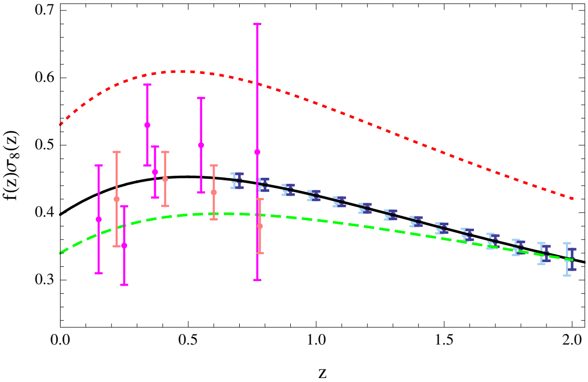

Forecasts of the errors expected on the growth rate (dark-blue error bars), expressed through the bias-free combination $f(z)\,\sigma_8(z)$, obtainable from the Euclid redshift survey[53]. The solid black line represents the fiducial $f(z)\,\sigma_8(z)$, computed for the standard cosmology, while the dashed green line shows the growth in a DGP model. The magenta and pink error bars are measurements from past and the recent WiggleZ survey.

[53] E. Majerotto *et al.*, arXiv:1205.6215 [astro-ph.CO].

Summary

- The six parameter base ΛCDM model continues to provide a very good match to the more extensive 2015 Planck data, including polarization. The 2015 Planck TT, TE, EE, and lensing spectra are consistent with each other under the assumption of the base ΛCDM cosmology.
- All of the BAO measurements are compatible with the base ΛCDM parameters from Planck[54].

[54] P. A. R. Ade *et al.*, arXiv:1502.01589 [astro-ph.CO].

Thank you for your attention